frontiers | Frontiers in Sustainable Food Systems

TYPE Original Research
PUBLISHED 27 August 2024
DOI 10.3389/fsufs.2024.1395730

OPEN ACCESS

EDITED BY
Shoomaila Latif,
University of the Punjab, Pakistan

REVIEWED BY
Swarup Roy,
Lovely Professional University, India
Allah Ditta,
Shaheed Benazir Bhutto University, Pakistan

*CORRESPONDENCE
Faiza Hassan
✉ faiza.hassan@chem.uol.edu.pk
Qamar uz Zaman
✉ qamar.zaman1@envs.uol.edu.pk

RECEIVED 04 March 2024
ACCEPTED 18 July 2024
PUBLISHED 27 August 2024

CITATION
Hassan F, Talib U, Saif S, Akhter P, Ali F, Abbas M, Younas U, Ashraf K, Alamri S and Zaman Qu (2024) Pectin functionalized with Cu/Fe nanoparticles for enhanced degradation of methylene blue from wastewater.
Front. Sustain. Food Syst. 8:1395730.
doi: 10.3389/fsufs.2024.1395730

Pectin functionalized with Cu/Fe nanoparticles for enhanced degradation of methylene blue from wastewater

Faiza Hassan[1]*, Usama Talib[1], Sadia Saif[1], Parveen Akhter[1], Faisal Ali[1], Moneeza Abbas[2], Umer Younas[1], Kamran Ashraf[3], Saud Alamri[4] and Qamar uz Zaman[5]*

[1]Department of Chemistry, The University of Lahore, Lahore, Pakistan, [2]Departments of Environmental Sciences, Lahore College for Women University, Lahore, Pakistan, [3]State Key Laboratory of Bioreactor Engineering, East China University of Science and Technology, Shanghai, China, [4]Department of Botany and Microbiology, College of Science, King Saud University, Riyadh, Saudi Arabia, [5]Department of Environmental Sciences, The University of Lahore, Lahore, Pakistan

Introduction: In the present study, citrus pectin-stabilized copper/iron bimetallic nanoparticle (NP) catalyst has been used for the degradation of methylene blue (MB) dye in wastewater produced from the food industry.

Methods: The P@Cu/Fe composites were synthesized by co-precipitation and the sol–gel methods.

Results and discussion: The characterization of the composites was carried out using UV, FTIR, SEM, and XRD techniques, revealing that P_1@Cu/FeNPs synthesized through co-precipitation had a particle size of 150–35 nm with an irregular spherical and hexagonal shape. P_2@Cu/FeNPs, synthesized using the gel combustion method using triethylamine as fuel, proved to be a better nanocatalyst with spherical particles having a uniform structure and size distribution of 105–23 nm. The mean zeta potential value of P_1@Cu/FeNPs was found to be between 0 and 5mv, showing the composite to be less stable and 13 mv for more stable P_2@Cu/FeNPs. The degradation of MB by P_1@Cu/FeNPs was recorded up to 23.57% after 35 min and the nanocomposite synthesized by the sol–gel method exhibited 97.28% degradation in 30 min. The P_2@Cu/FeNPs performed the best degradation due to their synergistic impact. In essence, this research represents a step toward the synthesis of bimetallic NPs using a biomaterial (citrus pectin) with improved synergistic photocatalytic potential that can induce different features in nanomaterials. Pectin-functionalized NPs using different metals should be synthesized and tested for different catalytic applications.

KEYWORDS

pectin, bimetallic nanoparticles, photocatalytic activity, methylene blue, nanocomposite

1 Introduction

In recent years, due to the rapid growth of industry, a huge amount of industrial waste are found to contain toxic dyes, heavy metals, and other harmful compounds that are being released into the environment. It has now become critical to remove dyes and heavy metals from wastewater in order to reduce the harmful effects of such effluents. The adsorption methods have currently received a lot of attention as a quick, inexpensive method

(Zeinali et al., 2014). One refractory contaminant that is frequently found in the effluent of various industries is MB (Mengting et al., 2020). According to the latest data, for 100,000 commercially dyed products, 7×10^5 tons of annually produced dyestuff are being released into aquatic environments. MB is a heterocyclic molecule identified as a cyanide and carbon monoxide antidote that is being used in the food industry for the testing of milk and dairy products. The presence of MB as a contaminant in water bodies has been reported to have detrimental effects on human health including irritation, nausea, diarrhea, dizziness, fever, and vomiting (Hamad and Idrus, 2022; Abuzeyad et al., 2024). MB prevents sunlight from entering the water body, which induces long-term effects on the ecosystem, harming aquatic life, and other living things. The basic structure of this particular dye consists of thiazine (Begum et al., 2017; Uddin et al., 2024). Such refractory pollutants have recently been investigated, and attempts have been made to remove these contaminants from wastewater using a variety of environmental technologies. The methods including Fenton's oxidation, electrochemical treatment, ion exchange, biological treatment, and adsorption have been reported for the degradation of dyes (Yanyan et al., 2018; Zhou et al., 2022).

Due to their distinct porous properties, activated carbon (Mercier et al., 2014), zeolites, and metal–organic frameworks have been reported to adsorb dyes in water treatment (Hamad and Idrus, 2022). Additionally, pectin or pectin-containing substances, such as fruit waste and macroalgae, can remove coloring agents (Bardakçı et al., 2014). The most promising and understudied field of research in the 21st century is nanotechnology. In many reports, the ability of nanomaterials has been reported for the treatment of wastewater containing dyes and nano-adsorbents, and NPs have shown great potential to advance wastewater treatment (Kumari et al., 2019; Abuzeyad et al., 2024). These nano-adsorbents have gained popularity because they are made of magnetic cores and polymeric shells that not only have a large specific surface area but can also be easily adjusted by an external magnetic field for separation convenience. The demands of removing significant volumes of dyes, however, cannot be achieved by simple adsorption. Adsorption combined with photocatalytic degradation is said to be a more successful dye removal method (Sarkar et al., 2012; Biftu et al., 2020). Pectin is a hydrocolloid polysaccharide formed by the binding and polymerization of galacturonic acid (GalA) with natural sugars by a glycoside bond (1–4) that is the main constituent of the cell walls of the plant. Most materialistic (commercial/industrial) pectin is extracted from the peels of citrus and the residue of apples, each of which is a byproduct of juice production (Wang et al., 2021). Its major applications are as a stabilizers in shampoo and a thickener in cosmetics and personal care products (Picot-Allain et al., 2022)..

Pectin molecules are flexible and open for modification purposes. The molecules carry a polyanion negative charge because of the ionization of the carboxyl group in their structure (Attallah et al., 2016). NPs of pectin are formed by the formation of intra-molecular and inter-molecular physical crosslinks and the existence of electrostatic interactions with the positively charged groups. Many divalent cations, such as $BaCl_2$, $MnCl_2$, and $ZnCl_2$, could be used for the pectin's gelation, and spherical-shaped NPs are formed. Pectin structure stabilizes this shape (form) by the electrostatic interaction of the carbonate (CO_3) anions with the crosslinking cations (Ergin et al., 2021). Due to their unique properties, such as high specific surface area, low thermal conductivity, high porosity, and relative density, pectin-based nanocomposites represent a novel approach in advanced food packing materials as they could be used as drug delivery systems, inner layers, and sensors (Ahmadzadeh et al., 2018; de Oliveira et al., 2019). It has been demonstrated through results that the bonding of carboxy groups of pectin with Cu^{+2} increased its adsorption capacity. The process was the preparation of pectin hydrogel with a low degree of esterification, which is why the adsorption capacity was strong on both Cu^{+2} and water. In addition to Cu^{+2}, the adsorption behavior of pectin hydrogel has been investigated kinetically and thermodynamically (Shen et al., 2022). Physical and chemical adsorptions were the results of the Cu^{+2} adsorption of hydrogel that was endothermic under natural conditions and favorable spontaneous adsorption led by the higher temperature (Saraf et al., 2016). Pectin has been used as an adsorbent, and NPs (CuS and CdS) served as the photocatalyst for the photocatalytic degradation of MB dye from wastewater under sunlight and lamp sources (Zhao and Zhou, 2016). The pectin@zirconium (IV) silicophosphate nanocomposite (Pc/ZSPNC) ion exchanger was synthesized by the sol–gel process, and a fine particle size was obtained. In the presence of sun radiation, Pc/ZSPNC displayed enhanced capacity and catalytic activity for the degradation of the MB dye. After 60 min of radiation exposure, 97.02% of the MB dye was found to be removed (Pathania et al., 2015). Pectin, a natural biopolymer, was used for the synthesis of PdNPs. Size-controlled PdNPs with a smaller size of 27.9 nm were generated at 70°C. Estimating catalytic efficiency in the discoloration of azo dye confirmed the catalytic potency of PdNPs prepared from pectin due to their greater surface area. Only 15 min were necessary for the degradation of the dye (Emam et al., 2020). A biopolymer pectin-graphene oxide (Pc/GO) nanocomposite was synthesized, and its effectiveness in photocatalytically degrading organic pollutants, including MB and methyl orange (MO) dyes, as well as the adsorptive removal of Cr (III) ions, was examined (Kaushal et al., 2020). A cross-linked copolymer network (Pec-g-PAMPS) was produced by free radical polymerization of a combination of 2-acrylamido-2-methylpropanesulfonic acid and pectin in the presence of N,N-methylenebisacrylamide. Using trisodium citrate to reduce silver nitrate inside the gel network, silver NPs were prepared and stabilized. MB removal from an aqueous solution using the hydrogel and the nanocomposite hydrogel was assessed using various methodologies (Baran, 2018). It has been found that Ag NPs significantly improve the Pec-g-PAMPS gels' capacity to swell. After 3 cycles, the nanocomposite hydrogel maintained 80% of its efficiency, demonstrating its reusability for wastewater treatment (Babaladimath and Badalamoole, 2019).

Using a simple chemical precipitation method, pectin-MnO_2 and pectin SnO_2 nanocomposites were created. Under various experimental circumstances, the prepared nanocomposite was used as a catalyst for the oxidative breakdown of calmagiten, an azoic dye. Under various conditions, the pectin-MnO_2 nanocomposite/H_2O_2 system completely degraded the calmagite solution (Jabli et al., 2023). The Cu/FeNPs in the presence of hydrogen peroxide (H_2O_2) can catalyze a Fenton-like reaction. Fe_2O_3 and H_2O_2 combine in this process to form hydroxyl radicals (•OH), which are extremely reactive and capable of breaking down organic contaminants such as MB (Wang et al., 2016; Yang et al., 2019). Natural polysaccharide pectin offers functional groups (such as carboxyl and hydroxyl) that improve MB molecule binding onto the NPs' surface. As a result, the MB concentration around the reactive sites increases. In addition to helping with adsorption, pectin stabilizes the NPs, keeping them from aggregating and preserving their high surface area and reactivity (Khodamorady and Bahrami, 2019).

Herein, the formation of novel hybrid composites of pectin has been carried out using cost-effective and eco-friendly precipitation and sol–gel methods. The main objective was to synthesize pectin biopolymer-based nanocomposites with a suitable pore size and the ability to maximize the degradation of MB dye. To the best of our knowledge, this study showed good results. Hence, this study will be an addition to the field of nanocomposite formation and an upgrade to the industrial use of their applications.

2 Materials and methods

2.1 Materials

Citrus pectin (98%), ferric chloride ($FeCl_3$) (99%), copper sulfate ($CuSO_4$) (99%), ethanol (98%), triethylamine (TEA) (98%), and sodium hydroxide (NaOH) (98%) were purchased from Sigma Aldrich. Wastewater samples containing MB were collected from the local food industry.

2.2 Synthesis of P_1@Cu/FeNPs

In order to fabricate P_1@Cu/FeNPs, an already reported co-precipitation method has been used (Figure 1). For this purpose, 0.4 M citrus pectin solution was made with 200 mL of distilled water, 0.1 M $FeCl_3$ (15 mL), and 0.1 M $CuSO_4$ (15 mL) were added in a conical flask, and stirred for 30 min at 60°C in the hot plate using a magnetic stirrer. NaOH solution was added to the mixture to obtain pH 3.5–4. As a result, the solution became concentrated, and a light greenish-brown jelly-type solution formed, indicating the formation of P_1@Cu/FeNPs nanocomposite (Doustkhah et al., 2018). The precipitates were kept in a drying oven for 6 h in a glass crucible for drying at 100°C. After drying, the precipitates were calcinated above 100°C (300–500°C) for 3 h (Younas et al., 2021).

2.3 Synthesis of P_2@Cu/FeNPs using the sol–gel method

An already reported sol–gel method was used for the synthesis of P_2@Cu/FeNPs (Figure 2). Shortly, 50 mL of triethylamine, 50 mL of ethanol, 200 mL of 0.4 M citrus pectin, 0.1 M of CuSO4 (50 mL), and 0.1 M solution of $FeCl_3$ (50 mL) were added in a conical flask and heated on a magnetic stirrer at 60°C for 30 min, with constant stirring. A very pungent odor was produced during this process. On removing from the hot plate and magnetic stirring, the solution was kept at room temperature to cool it down. A light brown colored gel was formed (Khashei et al., 2020; Bagherzade et al., 2021). The product was taken in a petri dish and heated at 300°C till the gel became brittle. The resulting material was crushed to fine particles with pestle mortar, and it resulted in P_2@Cu/FeNPs nanocomposite (Mehmood et al., 2022).

2.4 Characterization

The presence of different functional groups in P_1@Cu/FeNPs and P_2@Cu/FeNPs was evaluated with FTIR (BRUKER ALPHA-2). Crystallinity and phase composition of both composites were evaluated with X-ray diffraction (Bruker D8 Advance Eco) and morphology with field-emission scanning electron microscope (FE-SEM) (FEI Nova 450 NanoSEM). The catalytic performance results of samples were obtained with the help of a UV–visible spectrophotometer (CECIL 7400CE AQUARIUS).

2.5 Catalytic activity of P_1@Cu/FeNPs and P_2@Cu/FeNPs

The catalytic activity of P_1@Cu/FeNPs and P_2@Cu/FeNPs was investigated by a UV–visible spectrophotometer (CECIL 7400 CE AQUARIUS) in the scanning range of 200–800 nm. Each synthesized nanocomposite was sonicated in distilled water by using PG-215-Sonicator-017 for half an hour. Then 1 mL of the solution was taken in the test tube and covered the test tube with an aluminum foil sheet. The amount of MB measured in the wastewater solution was 0.03 mM. A dye sample was introduced into the test tube containing nanocomposite. The dye solution along with the nanocomposite sample was taken out from the solution mixture, and then the initial readings of the sample were recorded. After fixed intervals of time, readings were taken again (Nazir et al., 2022; Hassan et al., 2023). The degradation efficiency of the nanocomposites for the dye was determined with the help of the formula given below:

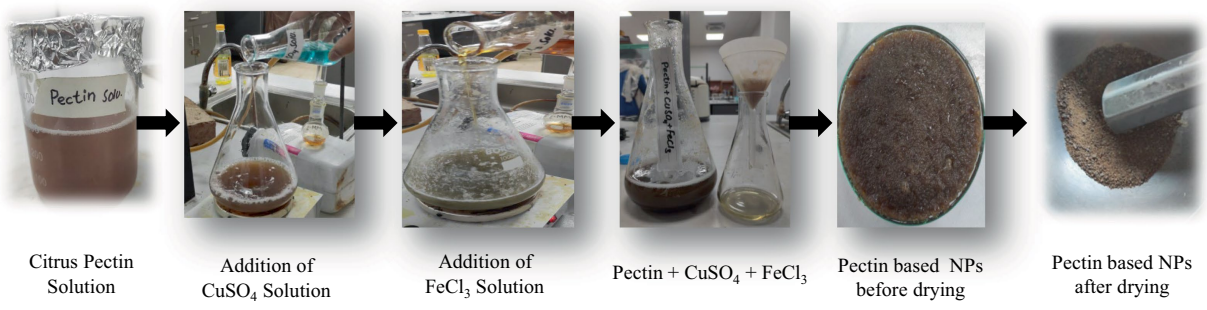

FIGURE 1
Synthesis of Cu/Fe bimetallic nanoparticles with citrus pectin (the co-precipitation method).

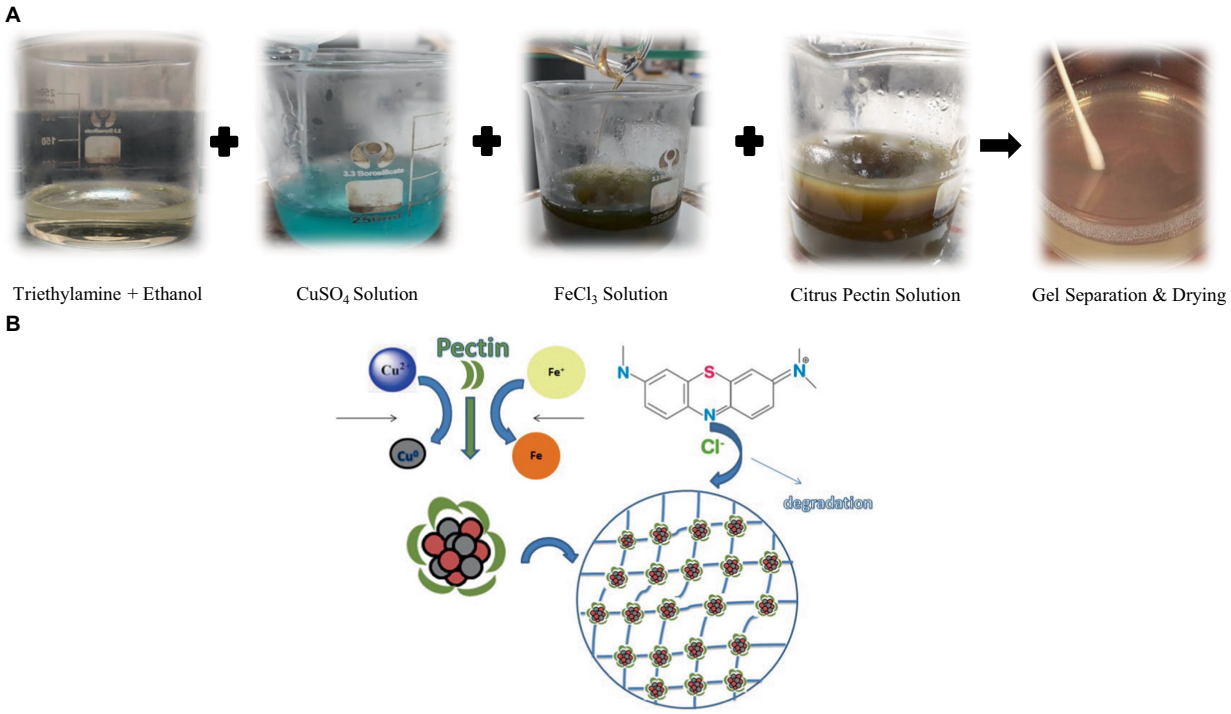

FIGURE 2
(A) Synthesis of Cu/Fe bimetallic nanoparticles with citrus pectin (the sol–gel method). **(B)** The mechanism of the formation of pectin functionalized Cu/FeNPs.

% Degradation = $(A_1{}^{-}A_t)/A_1 \times 100$.

Here, A_1 shows the initial absorbance of the solution containing dye along with the nanocomposite, and A_t shows absorbance at time "t" (Kaushal et al., 2020).

3 Results and discussion

3.1 Ultraviolet–visible spectroscopy

The absorbance of synthesized P_1@Cu/FeNPs by precipitated and P_2@Cu/FeNPs by the sol–gel method was recorded by UV–visible spectrophotometer (CECIL 7400 CE AQUARIUS) in the range of 200–800 nm. UV–vis spectrum P_1@Cu/FeNPs indicated λ_{max} value at 288 nm, which confirmed the presence of Fe metal (Latha and Gowri, 2014). The λ_{max} at 418 nm indicated the presence of citrus pectin, while λ_{max} at 578 nm confirmed Cu metal attachment to the nanostructure (Figure 3A). The spectrum for P_2@Cu/FeNPs shown in Figure 3B indicated a slight shift in the values of the λ_{max} with much sharper peaks but the ranges proved the presence of the same metals and groups, i.e., λ_{max} at 286 nm for Fe metal, 414 nm for citrus pectin, and 586 nm for Cu metal attached to the nanostructure (Rahman et al., 2019; Ghamari Kargar et al., 2022).

3.2 FTIR spectroscopy

The presence of functional groups and association with NPs were assessed in our samples by FTIR spectrophotometer (BRUKER ALPHA-2), and the results for both synthesized nanocomposite P_1@Cu/FeNPs and P_2@Cu/FeNPs are presented in Figures 4A–C. Mostly, the acid -OH broad peak overlapped with the -CH peak, which identified the acid. FTIR spectrum of citrus pectin can be seen in Figure 4A, which indicates the broad hydroxyl group peak for acids at 3322.51 cm^{-1} that is closely spaced to -CH stretching vibrational band located at 2940.22 cm^{-1}. The stretching peaks related to the carbonyl group (C=O) in the free carboxylic acid group are indicated at 1609.33 cm^{-1} (asymmetric stretching) and 1436.33 cm^{-1} (symmetric stretching). The band at 1730.75 cm^{-1} ascribes the esterified carboxyl group (C=O) of $COOCH_3$. The C-O stretching band can be seen at 1049.52 cm^{-1} (Chylińska et al., 2014).

The FTIR spectrum of P_1@Cu/FeNPs, as seen in Figure 4B, the broadband at 3255.24 cm^{-1} shows the hydroxyl group stretching of the acidic group, which is partially overlapped with the -CH stretching band (Sawant et al., 2016). The band is relatively stronger and weaker at 1615.85 cm^{-1} and 1437.11 cm^{-1}, which describes the carbonyl group (C=O) of the free carboxylic group. The band at 1733.07 cm^{-1} indicates the esterified carbonyl group of $COOCH_3$. The C-O stretching band was observed at 1012.17 cm^{-1} (Sharma and Jeevanandam, 2013). The shifting of the band from 3322.51 cm^{-1} to 3255.24 cm^{-1} shows evidence for the attachment of Cu- metal, and the appearance of a band at 632.42 cm^{-1} is due to the attachment of Fe metal to the pectin (Xue et al., 2021).

The FTIR spectrum of P_2@Cu/FeNPs is shown in Figure 4C. The band at 2978.44 cm^{-1} is mainly ascribed to the -CH stretch of -CH, $-CH_2$, and $-CH_3$ groups in the pectin structure, while the vibrational broadband at 3339.94 cm^{-1} describes the hydroxy group stretching of the acidic group, which is closely related to the -CH stretch band (Rana et al., 2019).

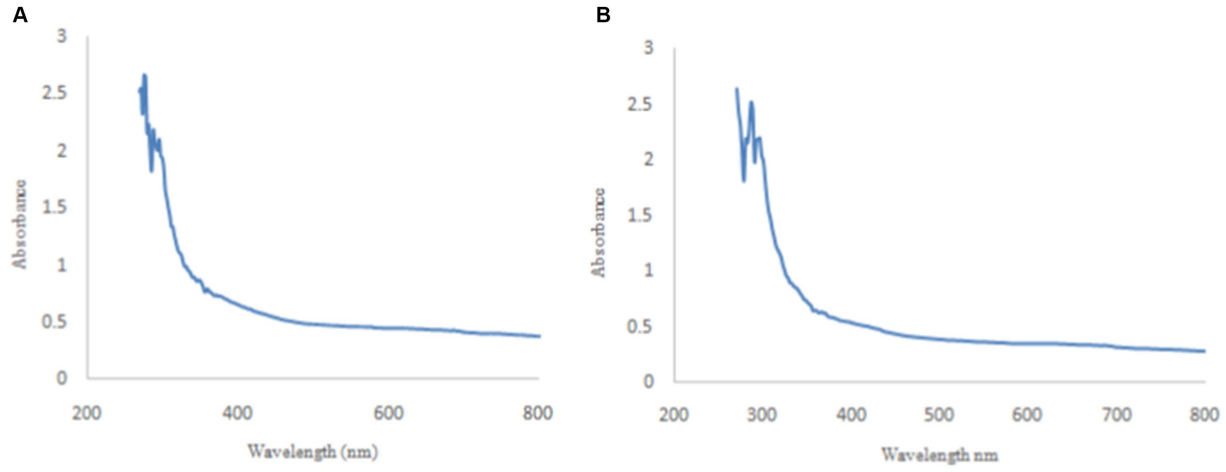

FIGURE 3
UV–vis spectrum of P_1@Cu/FeNPs **(A)** and P_2@Cu/FeNPs **(B)**.

The band attributed at 1625.76 cm^{-1} is associated with the asymmetric vibration of the carbonyl group, while the weaker band at 1475.15 cm^{-1} describes the symmetric vibration of the carbonyl group in the free carboxylic group. The peak at 1035.04 cm^{-1} indicates the C-O stretching. The appearance of bands at 3339.94 cm^{-1} and 807.02 cm^{-1} proved the formation of Fe-Cu bimetallic NPs of pectin (Xue et al., 2021). Finally, all the vibrational stretching bands of both samples are closely related to the reference pure citrus pectin (Khorasani and Shojaosadati, 2019).

3.3 X-ray diffractometry

The crystalline structures of both synthesized nanocomposites were determined by powder XRD. As shown in Figure 5B, it can be seen that the characteristic broad diffraction peaks for P_2@Cu/FeNPs shown in wide-angle XRD patterns can be indexed to the cubic spinal magnetite Fe crystal structure, which shows diffraction peaks; the patterns indicated a crystalline structure at 2θ: 32.3°, 43.6°, 54.8°, and 62.7°, which are assigned to (101), (220), (311), and (440) (Rana et al., 2019). Furthermore, the XRD pattern of the CuO can be seen in Figure 5A, indicating the peaks at 2θ: 36.82°, 46.73°, 58.02°, 62.47°, and 71.32° corresponding to the (110), (111), (202), (202), (220), and (222) crystallographic phases in the XRD pattern that are related to CuO. Much sharper and more prominent peaks at values approximately the same as in Figure 5B were observed in Figure 5A.

Low-angle XRD pattern of the P_1@Cu/FeNPs is also investigated and depicted in Figure 5A. The XRD pattern of both nanocomposites showed pronounced diffusion peaks from 20 to 30 that appeared due to pectin (Khashei et al., 2022). The XRD patterns of Fe and Cu immobilized on P_2@Cu/FeNPs show characteristic peaks whose relative intensities match well with the reported XRD of Fe_3O_4 magnetite and CuO (Nešić et al., 2018).

3.4 Scanning electron microscopy

The morphology of synthesized pectin-based nanocomposite by the precipitation method was analyzed by SEM and is shown in Figure 6A. SEM images of the sample represent the crystal structure of P_1@Cu/FeNPs as aggregated cubic-shaped particles. The particles with different diameters can be seen at a resolution of 200 nm, respectively. The diameter of pectin-based NPs was found to be 150 nm, 56 nm, and 32 nm. The results of the present study also agreed with the results of some previous studies (Zhang et al., 2013; Kurniawan et al., 2020). Similarly, the SEM images for P_2@Cu/FeNPs in Figure 6B represent the rhombic structured particles for 'Cu, as well as spherical particles for 'Fe' in large agglomerates of pectin-based nanocomposites (Lu, 2019; Li et al., 2022). The nanocomposites synthesized by the sol–gel method showed a clear size reduction with a diameter of 105 nm, 45 nm, and 23 nm at a resolution of 200 nm.

3.5 Photocatalytic activity

It has been demonstrated in recent research that natural polysaccharides can interact with dyes to provide a better binding capacity, which can be advantageous for the environment in the treatment of dye wastewater (Khodamorady and Bahrami, 2019). It can be seen in Table 1 that chitosan, cellulose, and pectin are the best adsorbents among other classes of polysaccharides. Chitosan doped with multiwalled carbon nanotubes and ZnO showed maximum %age degradation of MB (Malekkiani et al., 2022) in the case of chitosan-based adsorbents. Similarly, for cellulose, cellulose-carbon-doped TiO_2 (Habibi and Jamshidi, 2019) and for pectin, pectin-GO nanocomposite (Kaushal et al., 2020) showed the best results for the degradation of MB. The current study showed approximately the same results but in less time.

3.5.1 Photocatalytic activity of P_1@Cu/FeNPs

The spectrum for P_1@Cu/FeNPs (Figure 7A) confirmed that the wastewater containing dye was degraded by the synthesized NPs, and the decrease in absorbance proved the degradation of the dye (Gupta et al., 2015). The absorbance value of the reaction mixture containing synthesized NPs and MB (0.03 mM) at 664.5 nm was found to decrease after 15 min and 35 min. The decrease in absorbance confirmed the degradation of the dye and the percentage decrease was 14.86% after 15 min and 23.57% after 35 min (Ahmad and Ansari, 2021).

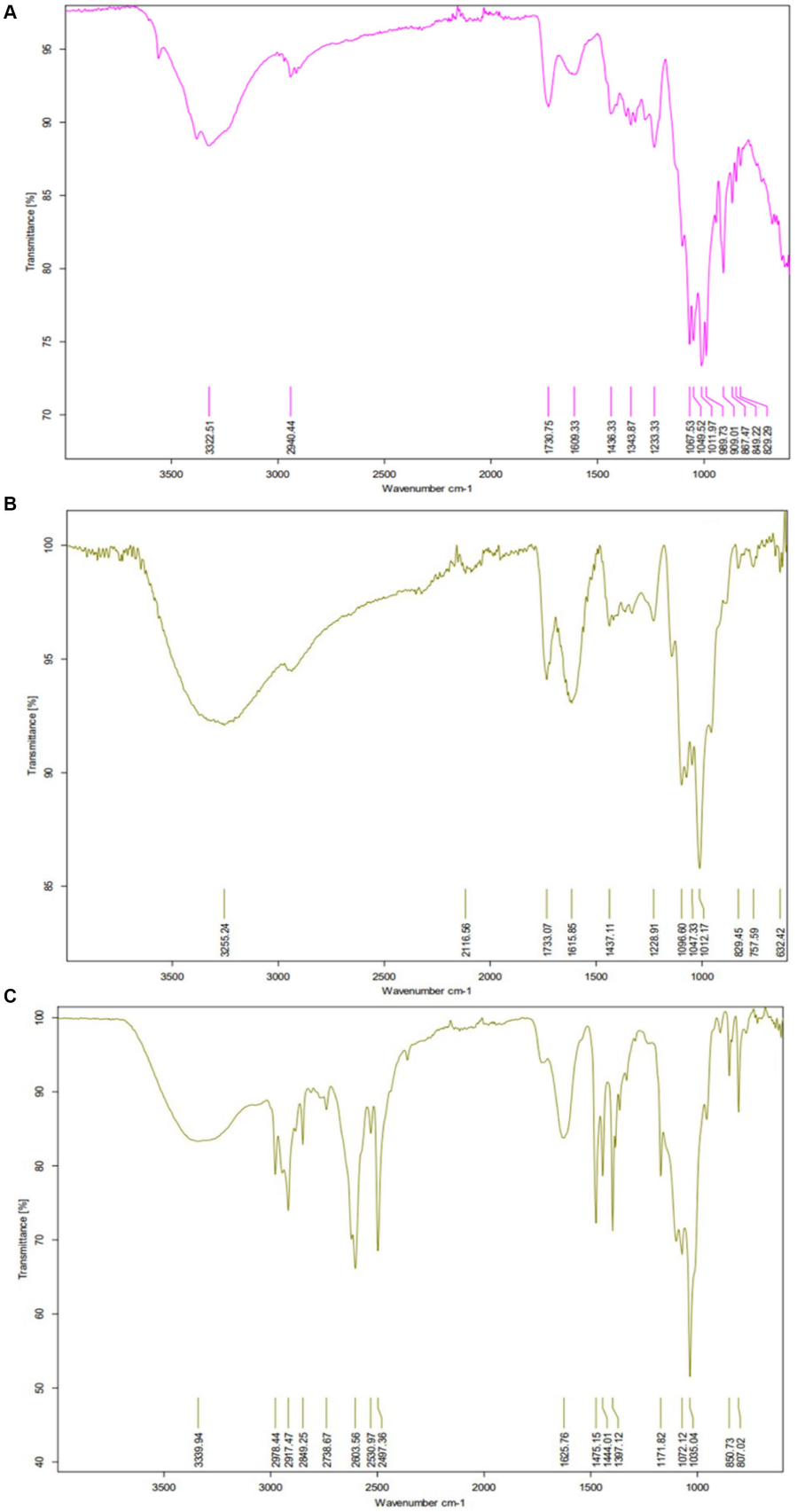

FIGURE 4
FTIR spectrum of pure Citrus Pectin **(A)**, P_1@Cu/FeNPs **(B)**, and P_2@Cu/FeNPs **(C)**.

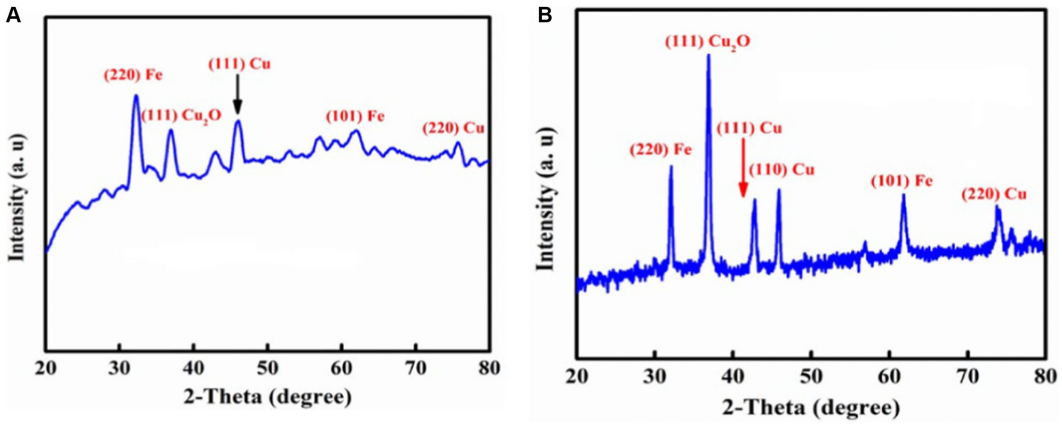

FIGURE 5
XRD pattern of P_1@Cu/FeNPs **(A)** and P_2@Cu/FeNPs **(B)**.

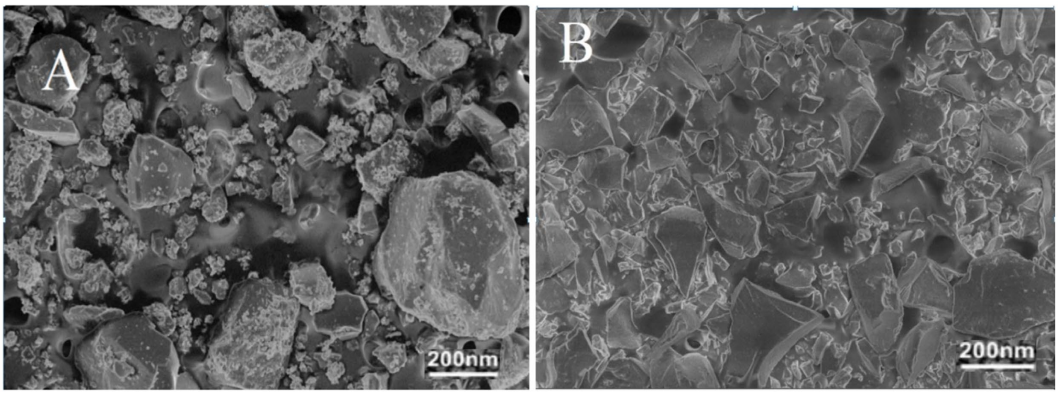

FIGURE 6
SEM images of P_1@Cu/FeNPs **(A)** and P_2@Cu/FeNPs **(B)** at 200 nm.

3.5.2 Photocatalytic activity of P_2@Cu/FeNPs

It can be noticed that from Figure 7B, for P_2@Cu/FeNPs, sharp peaks were obtained for the degradation process. Initially, P_2@Cu/FeNPs were allowed to react with MB (0.03 mM) wastewater sample, and the absorbance was recorded in terms of full wavelength scan. After 10-, 20-, and 30-min intervals, the value of absorbance was found to be continuously decreasing. The decrease in the value of absorbance at the same wavelength confirmed the degradation process for wastewater containing MB dye (Gupta et al., 2015). The percentage degradation of the dye in terms of absorbance was 20.81% after 10 min, 71.79% after 20 min, and 97.28% after 30 min. The maximum degradation of MB was observed in the case of P_2@Cu/FeNPs as compared to P_1@Cu/FeNPs.

As compared to the previous literature, P_2@Cu/FeNPs showed approximately the same percentage degradation as MWCNTs/ZnO/Chitosan (Malekkiani et al., 2022), cellulose-carbon doped TiO_2 (Habibi and Jamshidi, 2019), and pectin-GO nanocomposite (Kaushal et al., 2020), but in a very short time.

The Cu/FeNPs bonded to the citrus pectin's surface. When exposed to UV–vis light, the pollutant absorbs photons and becomes excited. The excited MB molecules then inject electrons into the NPs' conduction band, producing positive carbon radicals. $\cdot O_2^-$ and ·OH are formed when the electrons injected into the band interact with the O_2 adsorbed on the surface of CuO and iron oxide NPs (Kaushal et al., 2020). Positive carbon radicals in the dyes are attacked electrophilically by the reactive oxygen species ($\cdot O_2^-$), resulting in the formation of hydroxylated oxidation byproducts. The MB is then broken down into biodegradable oxidation byproducts, which are then adsorbed on the surface of citrus pectin (Nsom et al., 2019).

Cellulose-carbon doped TiO_2 (Habibi and Jamshidi, 2019), MWCNTs/ZnO/Chitosan (Malekkiani et al., 2022), and pectin-GO nanocomposite (Kaushal et al., 2020) showed enhanced degradation potential, as did the P_2@Cu/FeNPs, but in lesser time.

3.6 Zeta potential

The zeta potential of synthesized P_1@Cu/FeNPs by precipitated and P_2@Cu/FeNPs by the sol–gel method was recorded using Litesizer™ 500 particle analyzer in the range of −200 to +200 mv zeta potential distribution. The zeta potential for P_1@Cu/FeNPs in Figure 8A shows a distribution from −80 mv to +60 mv with the

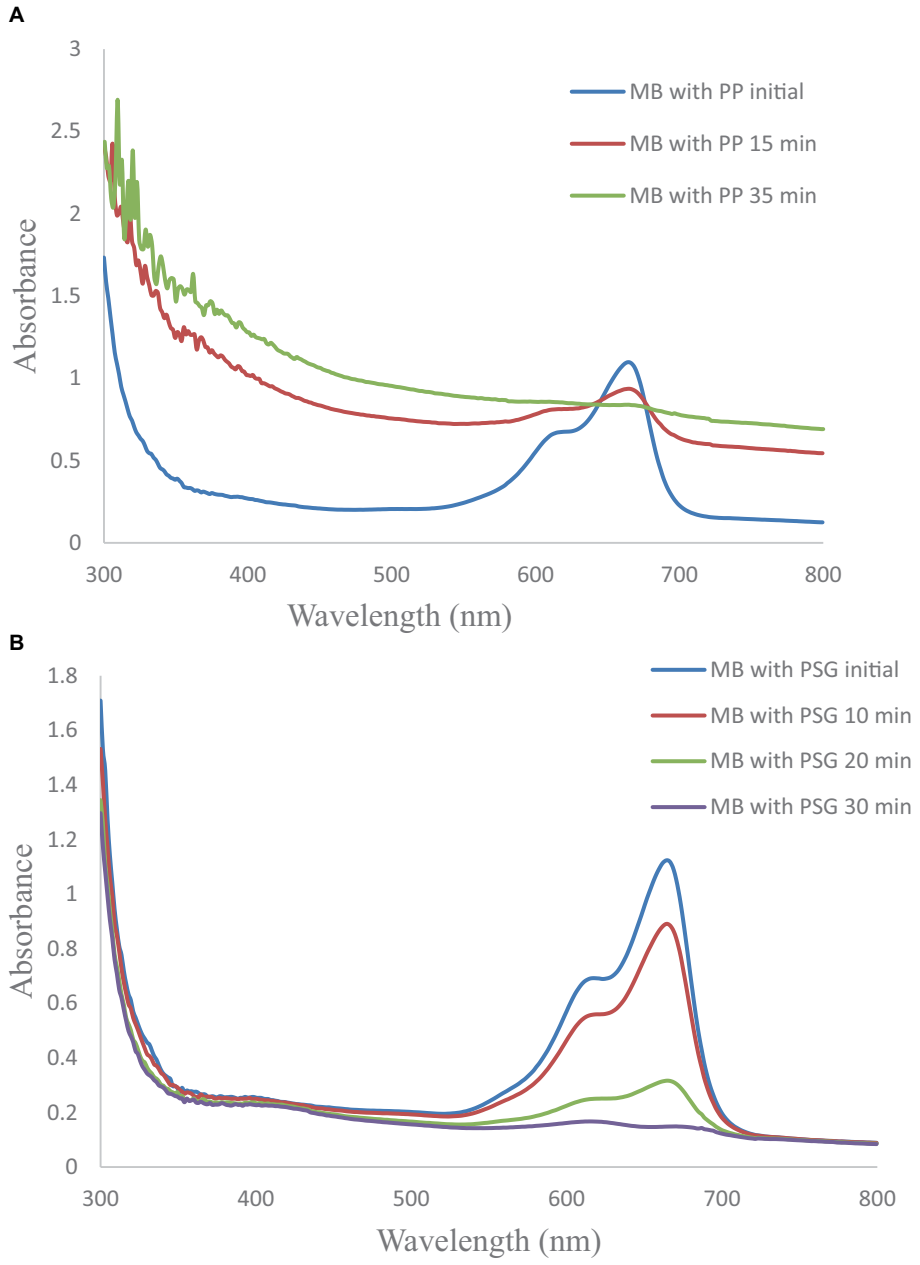

FIGURE 7
(A) Photocatalytic activity spectrum of P_1@Cu/FeNPs. **(B)** Photocatalytic activity spectrum of P_2@Cu/FeNPs.

mean zeta potential at zero, which confirmed the formation of electrical charges but was not very stable due to the mean value of 0 mv (Hodoroaba et al., 2019), and the value of +60 mv shows the stability of nanocomposites (Kumar et al., 2023). The zeta potential distribution for P_2@Cu/FeNPs shown in Figure 8B from −60 mv to 100 mv and a mean zeta potential of 13 mv indicated the formation of stable composites with variable charge distribution and dominance of positive charge of pectin-based Cu/FeNPs (Tabrizian et al., 2019). The larger the absolute value of ZP, the more chances there are for nanocomposite and nanoemulsion to repel and resist aggregate formation (Kumar et al., 2023).

3.7 Statistical data analysis

The adsorption experiments were repeated in triplicate. All the obtained data were analyzed. The data analyses were performed using Origin software (Table 2).

4 Conclusion

Cu/Fe bimetallic NPs were synthesized with citrus pectin through precipitation and the sol–gel methods successfully. The Cu/Fe was

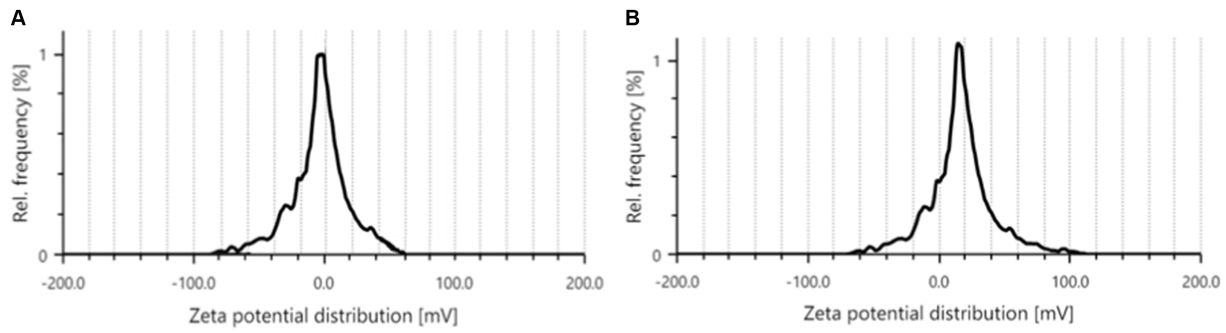

FIGURE 8
Zeta potential of P_1@Cu/FeNPs **(A)** and P_2@Cu/FeNPs **(B)**.

TABLE 1 Adsorption capacity of polysaccharide-related adsorbents for MB.

No	Adsorbents		Operating conditions	Maximum adsorption capacity (mg/g)/ percent	References
1	Starch	Starch stabilized iron NPs	pH = 3 reaction time = 30 min	300–100 mg/g	Dasgupta et al. (2022)
2		Starch-pectin-FeNPs	pH = 6–8 temp = 60°C–180°C	300–100 mg/g	Nsom et al. (2019)
3		Polyethyleneimine grafted starch nanocrystals	pH = 3–7 reaction time = 60 min	240.16–90.30 mg/g	Chen et al. (2021)
4	Chitosan	Chitosan-TiO_2	pH = 10–2 reaction time = 4 h	150 mg/g	Mahmoud et al. (2022)
5		Chitosan-ZnO_2-*Musa paradisiaca*	Reaction time = 1 h	90%	Roshitha et al. (2019)
6		Chitosan-MgO NPs	pH = 5–9 reaction time = 5–120 min	163.87 mg/g	Myneni et al. (2020)
7		MWCNTs/ZnO/Chitosan	pH = 5–9 reaction time = 20–180 min	97.8%	Malekkiani et al. (2022)
8	Cellulose	zinc oxide/cellulose nanocrystals	pH = 9 reaction time = 120 min	88.63%	Modi and Fulekar (2020)
9		Sawdust-cellulose-Zn NPs	pH = 2–10 reaction time = 0–500 min	64.93 mg/g	Oyewo et al. (2020)
10		Cellulose-carbon doped TiO_2	pH = 10 reaction time = 60–500 min	98%	Habibi and Jamshidi (2019)
11		Fe_3O_4@Cellulose Nanocomposite	pH = 2.5 reaction time = 0–60 min	69.7%	Lu (2019)
12	Pectin	Fe_3O_4-pectin NPs	pH = 5–10 reaction time = 0–400 min	141.3 mg/g	Zhang et al. (2016)
13		pectin-GO nanocomposite	pH = 2–7 reaction time = 25–90 min	98%	Kaushal et al. (2020)
14		Pectin-alginate- TiO_2 nanocomposite	pH = 4.27–4.48 reaction time = 0–30 min	435–637 mg/g	Zamri et al. (2021)
15		Pectin-Cu/Fe bimetallic nanocomposite	pH = 5–9 reaction time = 0–30 min	97.28%	Current study

TABLE 2 Percentage degradation of MB and kinetics of the reaction.

No	Reactions	Mean with standard error	Standard deviation
1	% deg. 7a MP with PP initial	73.49 ± 6.20	24.81
2	Kinetics 7a MP with PP initial	1.27 ± 0.107	0.430
3	% degradation 15 min	60.508 ± 4.88	19.54
4	Kinetics 15 min	1.474 ± 0.119	0.476
5	% deg. 35 min	50.45 ± 4.837	19.35
6	Kinetics 35 min	1.124 ± 0.107	0.431
7	% deg. 7b initial	73.81 ± 6.272	25.08
8	Kinetics Figure 7B initial	1.130 ± 0.096	0.384
9	% deg. 10 min	72.21 ± 6.402	25.60
10	Kinetics 10 min	1.106 ± 0.098	0.392
11	% deg. 20 min	79.33 ± 5.477	21.91
12	Kinetics 20 min	1.028 ± 0.071	0.284
13	% deg. 30 min	81.80 ± 5.694	22.77
14	Kinetics 30 min	1.100 ± 0.076	0.306

integrated into the surface of citrus pectin, and the association was confirmed from the UV–vis and FTIR spectra. The crystallinity of the citrus pectin was found due to the attachment of Cu/Fe and confirmed by XRD, and the change in morphology of both nanocomposites was proved by SEM analysis. Pectin-functionalized Cu/FeNPs promote the breakdown of MB through a combination of adsorption, catalytic degradation (Fenton-like and other redox processes), synergistic electron transfer, and surface complexation mechanisms. While the Cu and Fe components offer catalytic activity and effective electron transfer processes, the pectin coating boosts adsorption capacity and stability. Together, these mechanisms result in efficient and enhanced degradation of MB in wastewater treatment applications. Changes in the concentration of the dye were recorded in terms of absorbance, and wastewater containing MB became clear in the presence of the nanocomposite. It was further proved that the nanocomposites prepared through the sol–gel method gave better results as compared to those prepared by the co-precipitation method. In comparison with the previously reported studies, P_2@Cu/FeNPs showed a very good percentage for the absorbance of MB dye in a short time. Studies proved that nanocomposite synthesized by the sol–gel method can be an excellent candidate for the removal of organic dyes from food and textile industry wastewater.

Data availability statement

The original contributions presented in the study are included in the article/supplementary material, further inquiries can be directed to the corresponding authors.

Author contributions

FH: Conceptualization, Investigation, Methodology, Supervision, Writing – original draft. UT: Investigation, Writing – original draft. SS: Investigation, Writing – original draft. PA: Data curation, Resources, Writing – review & editing. FA: Validation, Writing – review & editing. MA: Data curation, Writing – review & editing. UY: Software, Writing – review & editing. KA: Investigation, Writing – original draft. SA: Investigation, Writing – original draft. QZ: Conceptualization, Investigation, Writing – review & editing.

Funding

The author(s) declare financial support was received for the research, authorship, and/or publication of this article. The authors sincerely acknowledge the Researchers Supporting Project number (RSP2024R194), King Saud University, Riyadh, Saudi Arabia.

Conflict of interest

The authors declare that the research was conducted in the absence of any commercial or financial relationships that could be construed as a potential conflict of interest.

Publisher's note

References

Abuzeyad, O. H., El-Khawaga, A. M., Tantawy, H., Gobara, M., and Elsayed, M. A. (2024). Photocatalytic Degradation of Methylene Blue Dye by Promising Zinc Copper Ferrite Nanoparticles for Wastewater Treatment. *Journal of Inorganic and Organometallic Polymers and Materials*. 1–11.

Ahmad, R., and Ansari, K. (2021). Enhanced sequestration of methylene blue and crystal violet dye onto green synthesis of pectin modified hybrid (Pect/AILP-Kal) nanocomposite. *Process Biochem.* 111, 132–143. doi: 10.1016/j.procbio.2021.10.009

Ahmadzadeh, S., Nasirpour, A., Keramat, J., and Desobry, S. (2018). "Powerful solution to mitigate the temperature variation effect: development of novel superinsulating materials" in Food packaging and preservation (London and Washington, DC: Academic Press), 137–176.

Attallah, O. A., Al-Ghobashy, M. A., Nebsen, M., and Salem, M. Y. (2016). Removal of cationic and anionic dyes from aqueous solution with magnetite/pectin and magnetite/silica/pectin hybrid nanocomposite: kinetic, isotherm and mechanism analysis. *RSC Adv.* 6, 11461–11480. doi: 10.1039/C5RA23452B

Babaladimath, G., and Badalamoole, V. (2019). Silver nanoparticles embedded pectin-based hydrogel: a novel adsorbent material for separation of cationic dyes. *Polym. Bull.* 76, 4215–4236. doi: 10.1007/s00289-018-2584-7

Bagherzade, G., Khashei Siuki, H., and Ghamari Kargar, P. (2021). Use of pectin as a suitable substrate for catalyst synthesis Fe3O4@ pectin@ Ni (II) and its application in oxidation reaction. *Medbiotech J.* 5, 1–8.

Baran, T. (2018). Pd (0) nanocatalyst stabilized on a novel agar/pectin composite and its catalytic activity in the synthesis of biphenyl compounds by Suzuki-Miyaura cross coupling reaction and reduction of o-nitroaniline. *Carbohydr. Polym.* 195, 45–52. doi: 10.1016/j.carbpol.2018.04.064

Bardakçı, B., Kalaycı, T., and Kınaytürk, N. K. (2014). Spectroscopic investigation of the adsorption of nitrophenol isomers on ammonium zeolite of type "Y". *Spectrosc. Lett.* 47, 621–629. doi: 10.1080/00387010.2013.836674

Begum, R., Yusof, Y. A., Aziz, M. G., and Uddin, M. B. (2017). Structural and functional properties of pectin extracted from jackfruit (*Artocarpus heterophyllus*) waste: effects of drying. *Int. J. Food Prop.* 20, S190–S201. doi: 10.1080/10942912.2017.1295054

Biftu, W. K., Ravindhranath, K., and Ramamoorty, M. (2020). New research trends in the processing and applications of iron-based nanoparticles as adsorbents in water remediation methods. *Nanotechnol. Environ. Eng.* 5, 1–12. doi: 10.1007/s41204-020-00076-y

Chen, Q., Zhao, Y., Xie, Q., Liang, C., and Zong, Z. (2021). Polyethyleneimine grafted starch nanocrystals as a novel biosorbent for efficient removal of methyl blue dye. *Carbohydr. Polym.* 273:118579. doi: 10.1016/j.carbpol.2021.118579

Chylińska, M., Szymańska-Chargot, M., and Zdunek, A. (2014). Imaging of polysaccharides in the tomato cell wall with Raman microspectroscopy. *Plant Methods* 10, 1–9. doi: 10.1186/1746-4811-10-14

Dasgupta, N., Nayak, M. A., and Gauthier, M. (2022). Starch-stabilized iron oxide nanoparticles for the photocatalytic degradation of methylene blue. *Polysaccharides* 3, 655–670. doi: 10.3390/polysaccharides3030038

de Oliveira, J. P., Bruni, G. P., El Halal, S. L. M., Bertoldi, F. C., Dias, A. R. G., and da Rosa Zavareze, E. (2019). Cellulose nanocrystals from rice and oat husks and their application in aerogels for food packaging. *Int. J. Biol. Macromol.* 124, 175–184. doi: 10.1016/j.ijbiomac.2018.11.205

Doustkhah, E., Heidarizadeh, M., Rostamnia, S., Hassankhani, A., Kazemi, B., and Liu, X. (2018). Copper immobilization on carboxylic acid-rich Fe3O4-pectin: Cu2+@ Fe3O4-pectin a superparamagnetic nanobiopolymer source for click reaction. *Mater. Lett.* 216, 139–143. doi: 10.1016/j.matlet.2018.01.014

Emam, H. E., Saad, N. M., Abdallah, A. E., and Ahmed, H. B. (2020). Acacia gum versus pectin in fabrication of catalytically active palladium nanoparticles for dye discoloration. *Int. J. Biol. Macromol.* 156, 829–840. doi: 10.1016/j.ijbiomac.2020.04.018

Ergin, A. D., Bayindir, Z. S., Ozcelikay, A. T., and Yuksel, N. (2021). A novel delivery system for enhancing bioavailability of S-adenosyl-l-methionine: pectin nanoparticles-in-microparticles and their in vitro-in vivo evaluation. *J. Drug Deliv. Sci. Technol.* 61:102096. doi: 10.1016/j.jddst.2020.102096

Ghamari Kargar, P., Ghasemi, M., and Bagherzade, G. (2022). Copper (II) supported on a post-modified magnetic pectin Fe3O4@ pectin~ imidazole~ SO3H-cu (II): an efficient biopolymer-based catalyst for selective oxidation of alcohols with aqueous TBHP. *Sci. Iranica* 29, 1338–1350.

Gupta, V. K., Sharma, G., Pathania, D., and Kothiyal, N. C. (2015). Nanocomposite pectin Zr (IV) selenotungstophosphate for adsorptional/photocatalytic remediation of methylene blue and malachite green dyes from aqueous system. *J. Ind. Eng. Chem.* 21, 957–964. doi: 10.1016/j.jiec.2014.05.001

Habibi, S., and Jamshidi, M. (2019). Sol–gel synthesis of carbon-doped TiO2 nanoparticles based on microcrystalline cellulose for efficient photocatalytic degradation of methylene blue under visible light. *Environ. Technol.* 41, 3233–3247. doi: 10.1080/09593330.2019.1604815

Hamad, H. N., and Idrus, S. (2022). Recent developments in the application of bio-waste-derived adsorbents for the removal of methylene blue from wastewater: a review. *Polymers* 14:783. doi: 10.3390/polym14040783

Hassan, F., Abbas, A., Ali, F., Nazir, A., Al Huwayz, M., Alwadai, N., et al. (2023). Bio-mediated synthesis of Cu-TiO_2 nanoparticles using *Phoenix dactylifera* lignocellulose as capping and reducing agent for the catalytic degradation of toxic dyes. *Desalin. Water Treat.* 298, 53–60. doi: 10.5004/dwt.2023.29613

Hodoroaba, V. D., Unger, W., and Shard, A. (2019). Characterization of nanoparticles: measurement processes for nanoparticles. Amsterdam, The Netherlands: Elsevier.

Jabli, M., Sebeia, N., and Bchetnia, A. (2023). Synthesis and characterization of pectin-manganese oxide and pectin-tin oxide nanocomposites: application to the degradation of calmagite in water. *J. Polym. Environ.* 31, 4326–4337. doi: 10.1007/s10924-023-02888-w

Kaushal, S., Kaur, N., Kaur, M., and Singh, P. P. (2020). Dual-responsive pectin/graphene oxide (pc/GO) nano-composite as an efficient adsorbent for Cr (III) ions and photocatalyst for degradation of organic dyes in waste water. *J. Photochem. Photobiol. A Chem.* 403:112841. doi: 10.1016/j.jphotochem.2020.112841

Khashei, S. H., Bagherzade, G., and Ghamari, K. P. (2020). A green method for synthesizing nickel nanoparticles supported by magnetized pectin: applied as a catalyst for aldehyde synthesis as a precursor in xanthan synthesis. *ChemistrySelect* 5, 13537–13544. doi: 10.1002/slct.202002946

Khashei, S. H., Ghamari, P., and Bagherzade, G. (2022). New Acetamidine cu (II) Schiff base complex supported on magnetic nanoparticles pectin for the synthesis of triazoles using click chemistry. *Sci. Rep.* 12:3771. doi: 10.1038/s41598-022-07674-7

Khodamorady, M., and Bahrami, K. (2019). Fe3O4@ BNPs-CPTMS-chitosan-Pd (0) as an efficient and stable heterogeneous magnetic nanocatalyst for the chemoselective oxidation of alcohols and homoselective synthesis of 5-subestituted 1H-tetrazoles. *ChemistrySelect* 4, 8183–8194. doi: 10.1002/slct.201901497

Khorasani, A. C., and Shojaosadati, S. A. (2019). Magnetic pectin-*Chlorella vulgaris* biosorbent for the adsorption of dyes. *J. Environ. Chem. Eng.* 7:103062. doi: 10.1016/j.jece.2019.103062

Kumar, M., Mohapatra, S., and Weber, K. (2023). Emerging aquatic contaminants: one health framework for risk assessment and remediation in the post COVID-19 anthropocene. Amsterdam, The Netherlands: Elsevier.

Kumari, P., Alam, M., and Siddiqi, W. A. (2019). Usage of nanoparticles as adsorbents for waste water treatment: an emerging trend. *Sustain. Mater. Technol.* 22:e00128. doi: 10.1016/j.susmat.2019.e00128

Kurniawan, T. A., Mengting, Z., Fu, D., Yeap, S. K., Othman, M. H. D., Avtar, R., et al. (2020). Functionalizing TiO2 with graphene oxide for enhancing photocatalytic degradation of methylene blue (MB) in contaminated wastewater. *J. Environ. Manag.* 270:110871. doi: 10.1016/j.jenvman.2020.110871

Latha, N., and Gowri, M. (2014). Biosynthesis and characterisation of Fe3O4 nanoparticles using Caricaya papaya leaves extract. *Int. J. Sci. Res.* 3, 1551–1556.

Li, H., Xu, C., Li, N., Rao, T., Zhou, Z., Zhou, Q., et al. (2022). Synthesis of bimetallic FeCu-MOF and its performance as catalyst of peroxymonosulfate for degradation of methylene blue. *Materials* 15:7252. doi: 10.3390/ma15207252

Lu, Q. (2019). In situ synthesis of a stable Fe3O4@ cellulose nanocomposite for efficient catalytic degradation of methylene blue. *Nano* 9:275. doi: 10.3390/nano9020275

Mahmoud, G. A., Sayed, A., Thabit, M., and Safwat, G. (2022). Chitosan biopolymer based nanocomposite hydrogels for removal of methylene blue dye. *SN Appl. Sci.* 2:968. doi: 10.1007/s42452-020-2753-9

Malekkiani, M., Heshmati Jannat Magham, A., Ravari, F., and Dadmehr, M. (2022). Facile fabrication of ternary MWCNTs/ZnO/Chitosan nanocomposite for enhanced photocatalytic degradation of methylene blue and antibacterial activity. *Sci. Rep.* 12:5927. doi: 10.1038/s41598-022-09571-5

Mehmood, F., Kousar, H., Hassan, F., and Zaman, Q. U. (2022). Synthesis of zinc oxide nanoparticles by precipitation and sol gel methods from different precursors and their comparison impact on seedling attributes of wheat. *J. Nano Res.* 72, 25–35. doi: 10.4028/p-2sa57f

Mengting, Z., Tonni, A. K., You, Y., Mohd, H. D. O., Ram, A., Dun, F., et al. (2020). Fabrication, characterization, and application of ternary magnetic recyclable Bi2WO6/BiOI@ Fe3O4 composite for photodegradation of tetracycline in aqueous solutions. *J. Environ. Manag.* 270:110839. doi: 10.1016/j.jenvman.2020.110839

Mercier, A., Joulian, C., Michel, C., Auger, P., Coulon, S., Amalric, L., et al. (2014). Evaluation of three activated carbons for combined adsorption and biodegradation of PCBs in aquatic sediment. *Water Res.* 59, 304–315. doi: 10.1016/j.watres.2014.04.021

Modi, S., and Fulekar, M. H. (2020). Synthesis and characterization of zinc oxide nanoparticles and zinc oxide/cellulose nanocrystals nanocomposite for photocatalytic degradation of methylene blue dye under solar light irradiation. *Nanotechnol. Environ. Eng.* 5, 1–12. doi: 10.1007/s41204-020-00080-2

Myneni, V. R., Kanidarapu, N. R., and Vangalapati, M. (2020). Methylene blue adsorption by magnesium oxide nanoparticles immobilized with chitosan (CS-MgONP): response surface methodology, isotherm, kinetics and thermodynamic studies. *Iran. J. Chem. Chem. Eng.* 39, 29–42. doi: 10.30492/ijcce.2019.36342

Nazir, A., Zahid, S., Mahmood, Z., Kanwal, F., Latif, S., Imran, M., et al. (2022). Adsorption kinetics for the removal of toxic Congo red dye by polyaniline and citrus leaves as effective adsorbents. *Z. Phys. Chem.* 236, 1301–1319. doi: 10.1515/zpch-2022-0014

Nešić, A., Gordić, M., Davidović, S., Radovanović, Ž., Nedeljković, J., Smirnova, I., et al. (2018). Pectin-based nanocomposite aerogels for potential insulated food packaging application. *Carbohydr. Polym.* 195, 128–135. doi: 10.1016/j.carbpol.2018.04.076

Nsom, M. V., Etape, E. P., Tendo, J. F., Namond, B. V., Chongwain, P. T., Yufanyi, M. D., et al. (2019). A green and facile approach for synthesis of starch-pectin magnetite nanoparticles and application by removal of methylene blue from textile effluent. *J. Nanomater.* 2019, 1–12. doi: 10.1155/2019/4576135

Oyewo, O. A., Adeniyi, A., Sithole, B. B., and Onyango, M. S. (2020). Sawdust-based cellulose nanocrystals incorporated with ZnO nanoparticles as efficient adsorption media in the removal of methylene blue dye. *ACS Omega* 5, 18798–18807. doi: 10.1021/acsomega.0c01924

Pathania, D., Sharma, G., and Thakur, R. (2015). Pectin@ zirconium (IV) silicophosphate nanocomposite ion exchanger: photo catalysis, heavy metal separation and antibacterial activity. *Chem. Eng. J.* 267, 235–244. doi: 10.1016/j.cej.2015.01.004

Picot-Allain, M. C. N., Ramasawmy, B., and Emmambux, M. N. (2022). Extraction, characterisation, and application of pectin from tropical and sub-tropical fruits: a review. *Food Rev. Intl.* 38, 282–312. doi: 10.1080/87559129.2020.1733008

Rahman, T., Borah, G., and Gogoi, P. K. (2019). Hybrid composite of CuO with g-C _ 3 N _ 4 g-C 3 N 4 as a photoactive catalyst: an efficient approach for the oxidation of alcohols. *J. Chem. Sci.* 131, 1–9. doi: 10.1007/s12039-018-1581-6

Rana, P., Sharma, S., Sharma, R., and Banerjee, K. (2019). Apple pectin supported superparamagnetic (γ-Fe2O3) maghemite nanoparticles with antimicrobial potency. *Mater. Sci. Energy Technol.* 2, 15–21. doi: 10.1016/j.mset.2018.09.001

Roshitha, S. S., Mithra, V., Saravanan, V., Sadasivam, S. K., and Gnanadesigan, M. (2019). Photocatalytic degradation of methylene blue and safranin dyes using chitosan zinc oxide nano-beads with Musa× paradisiaca L. pseudo stem. *Bioresource Technol. Rep.* 5, 339–342. doi: 10.1016/j.biteb.2018.08.004

Saraf, M., Natarajan, K., and Mobin, S. M. (2016). Non-enzymatic amperometric sensing of glucose by employing sucrose templated microspheres of copper oxide (CuO). *Dalton Trans.* 45, 5833–5840. doi: 10.1039/C6DT00670A

Sarkar, S., Guibal, E., Quignard, F., and SenGupta, A. K. (2012). Polymer-supported metals and metal oxide nanoparticles: synthesis, characterization, and applications. *J. Nanopart. Res.* 14, 1–24. doi: 10.1007/s11051-011-0715-2

Sawant, S. S., Bhagwat, A. D., and Mahajan, C. M. (2016). Novel facile technique for synthesis of stable cuprous oxide (Cu2O) nanoparticles–an ageing effect. *J. Nano Electron. Phys.* 8:01036. doi: 10.21272/jnep.8(1).01036

Sharma, G., and Jeevanandam, P. (2013). Synthesis of self-assembled prismatic iron oxide nanoparticles by a novel thermal decomposition route. *RSC Adv.* 3, 189–200. doi: 10.1039/C2RA22004K

Shen, B., Guo, Z., Huang, B., Zhang, G., Fei, P., and Hu, S. (2022). Preparation of hydrogels based on pectin with different esterification degrees and evaluation of their structure and adsorption properties. *Int. J. Biol. Macromol.* 202, 397–406. doi: 10.1016/j.ijbiomac.2021.12.160

Tabrizian, P., Ma, W., Bakr, A., and Rahaman, M. S. (2019). pH-sensitive and magnetically separable Fe/cu bimetallic nanoparticles supported by graphene oxide (GO) for high-efficiency removal of tetracyclines. *J. Colloid Interface Sci.* 534, 549–562. doi: 10.1016/j.jcis.2018.09.034

Uddin, J., Idrees, M., Ahmed, H., Batool, S., Rahman, T. U., Mehmood, S., et al. (2024). Biodegradation and decolorization of methylene blue, reactive Black-5, and toluidine blue-O from an aqueous solution using the polyphenol oxidase enzyme. *Front. Sustain. Food Syst.* 7:1320855. doi: 10.3389/fsufs.2023.1320855

Wang, C., Qiu, W. Y., Chen, T. T., and Yan, J. K. (2021). Effects of structural and conformational characteristics of citrus pectin on its functional properties. *Food Chem.* 339:128064. doi: 10.1016/j.foodchem.2020.128064

Wang, N., Zheng, T., Zhang, G., and Wang, P. (2016). A review on Fenton-like processes for organic wastewater treatment. *J. Environ. Chem. Eng.* 4, 762–787. doi: 10.1016/j.jece.2015.12.016

Xue, W., Yang, G., Karmakar, B., and Gao, Y. (2021). Sustainable synthesis of Cu NPs decorated on pectin modified Fe3O4 nanocomposite: catalytic synthesis of 1-substituted-1H-tetrazoles and in-vitro studies on its cytotoxicity and anti-colorectal adenocarcinoma effects on HT-29 cell lines. *Arab. J. Chem.* 14:103306. doi: 10.1016/j.arabjc.2021.103306

Yang, W., Yuen, A. C. Y., Ping, P., Wei, R. C., Hua, L., Zhu, Z., et al. (2019). Pectin-assisted dispersion of exfoliated boron nitride nanosheets for assembled bio-composite aerogels. *Compos. A: Appl. Sci. Manuf.* 119, 196–205. doi: 10.1016/j.compositesa.2019.02.003

Yanyan, L., Kurniawan, T. A., Zhu, M., Ouyang, T., Avtar, R., Othman, M. H. D., et al. (2018). Removal of acetaminophen from synthetic wastewater in a fixed-bed column adsorption using low-cost coconut shell waste pretreated with NaOH, HNO3, ozone, and/or chitosan. *J. Environ. Manag.* 226, 365–376. doi: 10.1016/j.jenvman.2018.08.032

Younas, U., Hassan, S. T., Ali, F., Hassan, F., Saeed, Z., Pervaiz, M., et al. (2021). Radical scavenging and catalytic activity of Fe-Cu bimetallic nanoparticles synthesized from *Ixora finlaysoniana* extract. *Coatings* 11:813. doi: 10.3390/coatings11070813

Zamri, N. I. I., Zulmajdi, S. L. N., Daud, N. Z. A., Mahadi, A. H., Kusrini, E., and Usman, A. (2021). Insight into the adsorption kinetics, mechanism, and thermodynamics of methylene blue from aqueous solution onto pectin-alginate-titania composite microparticles. *SN Appl. Sci.* 3, 1–16. doi: 10.1007/s42452-021-04245-9

Zeinali, N., Ghaedi, M., and Shafie, G. (2014). Competitive adsorption of methylene blue and brilliant green onto graphite oxide nano particle following: derivative spectrophotometric and principal component-artificial neural network model methods for their simultaneous determination. *J. Ind. Eng. Chem.* 20, 3550–3558. doi: 10.1016/j.jiec.2013.12.048

Zhang, Q., Li, J., Chou, X., Gao, L., Hai, Z., and Xue, C. (2013). Synthesis of superparamagnetic iron oxide nanoparticles in carbon reduction method. *Micro Nano Lett.* 8, 598–601. doi: 10.1049/mnl.2013.0364

Zhang, W., Zhang, L. Y., Zhao, X. J., and Zhou, Z. (2016). Citrus pectin derived ultrasmall Fe3O4@ C nanoparticles as a high-performance adsorbent toward removal of methylene blue. *J. Mol. Liq.* 222, 995–1002. doi: 10.1016/j.molliq.2016.07.144

Zhao, X. J., and Zhou, Z. Q. (2016). Synthesis and applications of pectin-based nanomaterials. *Curr. Nanosci.* 12, 103–109. doi: 10.2174/1573413711666150818224020

Zhou, Y., Lin, M., Liu, C., Wang, L., Chen, H., Dan, C., et al. (2022). Enhancing mechanical properties of uniformly distributed nano TiB2/2024 Al composite rolling sheet by pre-stretch aging. Journal of Alloys and Compounds. 913: 165172